Bulletin of the Seismological Society of America, Vol. 92, No. 8, pp. 3006–3021, December 2002

Stochastic Fault Stress: Implications for Fault Dynamics and Ground Motion

by David D. Oglesby and Steven M. Day

Abstract Up to the present time, ground-motion calculations for future earthquakes have almost exclusively been made from kinematic models. However, dynamic faulting models offer many benefits over kinematic models, including the assurance the faulting models obey at least the general rules of elastodynamics and friction and contain a natural relationship between stress drop, slip, rise time, and rupture velocity. Dynamic models also offer insight into the physics of the rupture and slip processes and can show how these processes lead to patterns of ground motion. In the current work, we use the 3D finite-difference method and a suite of stochastic stress patterns, with variable assumptions on strength and stress inhomogeneity, to investigate two issues: (1) the effect of assumptions about stress pattern on the evolution of rupture and slip on the fault, and (2) the effect of these assumptions on the resultant ground motion. We find that stress drop has a complicated relationship with slip, rise time, and rupture velocity, especially in faults with strongly heterogeneous strength. We also find that these inhomogeneous-strength faults can produce highly inhomogeneous slip, even without any form of frictional restrengthening at healing time. Finally, we find that smoother strength models produce a better fit than the coarse models to the directivity pulse often observed on the surface. The results help to shed light on the transition of the faulting system between locally controlled and more globally controlled rupture and also show how dynamic models may be used to generate ground-motion estimates for seismic hazard calculations.

Introduction

In principle, if seismologists had unlimited information on fault geometry, fault stress, frictional properties, and material properties, prediction of ground motion in future earthquakes could possibly be a tractable task. However, our knowledge of the source, site, and path is often very limited, and we are forced to make many assumptions about these physical quantities in order to model earthquakes. In particular, the state of stress on a fault clearly has a very large effect on both the physics of the earthquake process and the resultant ground motion. Unfortunately, the state of stress on a fault prior to an earthquake is largely unknown, and this fact has led to numerous different *a priori* assumptions in faulting models. Kinematic models often assume some sort of stochastic rupture time and slip distribution on the fault. With many different simulations, a wide spectrum of ground motion may be obtained for seismic hazard analysis. A difficulty with such models is that there is no guarantee that such rupture patterns are physically plausible—the parameter space is not necessarily constrained to the subspace of physically realizable scenarios. In particular, stochastic kinematic models often consider slip, slip duration (rise time), and rupture time to be uncorrelated, whereas in nature it is quite likely that they are correlated, albeit in perhaps complex ways. In contrast, dynamic models assure that the faulting models obey certain physical laws (elasticity and friction), but uncertainties in the nature of the frictional law and fault stress persist. In the current study, we perform dynamic rupture simulations using stochastic stress patterns. Our goals are (1) to explore systematically the effect on rupture dynamics of different assumptions about fault stress and strength, and (2) to show how the fault dynamics affects ground-motion predictions for seismic hazard purposes. Our main results include a complicated relationship between slip, rupture velocity, and rise time, especially on faults with inhomogeneous strength properties. In these cases of highly inhomogeneous fault strength, heterogeneous slip does not require slip rate weakening and is present in slip-weakening models. In addition, we find that the often-observed directivity pulse is more prominent in earthquakes with smoother strength distributions, even when the stress drop is highly inhomogeneous. These results could help to constrain the types of stress fields that lead to realistic ground motion and

suggest that dynamic models can produce useful ground-motion results for seismic hazard analysis.

Dynamic earthquake rupture models have begun to be more commonplace as computational power and numerical techniques have advanced, and recent works have help to elucidate the interdependence of the stress pattern, slip, and rupture propagation under various circumstances. Day (1982) was the first to study in detail the full three-dimensional problem of spontaneous fault rupture, using a slip-weakening friction law and inhomogeneous prestress. He found that variations in rupture velocity were strongly linked to variations in the prestress pattern on the fault and that supershear rupture velocity was locally possible, even if the average rupture velocity was subshear. High slip velocity was also strongly correlated with areas of maximum shear prestress and fast rupture velocity. Fukuyama and Madariaga (2000) investigated a similar physical situation and found that smaller-scale stress heterogeneity did not lead to super-shear rupture velocities but led to a weaker relationship between prestress and rupture velocity. Other studies have attempted to investigate the effects of fault stress and ground motion in the context of fitting data from recent earthquakes. Of particular importance for the present work is the issue of how to produce the slip heterogeneity and short rise times inferred in faulting models for recent events. Heaton (1990), has argued that a rate-weakening friction law (which thus includes a form of frictional restrengthening) is the simplest explanation for these effects. However, Beroza and Mikumo (1996), in their dynamic model for the 1984 Morgan Hill earthquake, found that they could explain the short rise times and slip heterogeneity with no rate weakening in their friction law. Olsen *et al.* (1997) and Nielsen and Olsen (2000) have constructed dynamic models for the 1992 Landers and 1994 Northridge earthquakes, respectively. Their results showed that it was quite difficult to produce faulting models that would fit the desired slip patterns while still propagating over the entire fault plane—the results were very sensitive to the slip-weakening distance, connectivity of high-stress patches, and the degree of rate weakening. The current study examines this issue in detail to capture the transition of a system from one of relatively easy rupture propagation to one in which propagation is relatively improbable. It also investigates the dependence of slip heterogeneity on the assumptions of stress and strength heterogeneity.

In addition to gaining insight on earthquake physics from first-principles models and recent earthquakes, another issue in earthquake modeling is the synthesis of realistic ground motion for future earthquakes. This task is of crucial importance in seismic hazard calculation and is traditionally accomplished by kinematic models, which are in turn based on slip models of previous earthquakes. However, as argued previously, such kinematic models are not necessarily physically realizable, leading to an overly large parameter space where the connections among slip, rupture velocity, and rise time are assumed, not calculated. Mai *et al.* (2001) have performed and examined the results from many dynamic earthquake models with stochastic prestress stress patterns to arrive at a scheme for constructing more realistic kinematic rupture models. This article also examines the results from stochastic stress patterns, with a specific emphasis on examining the sensitivity of the rupture dynamics and ground motion to assumptions about the fault strength.

Method

Earthquake Scenario

Current computational capabilities permit ground motion to be simulated from 3D spontaneous rupture models at a spatial scale and frequency bandwidth of practical interest. To emphasize the potential of spontaneous rupture models to address practical earthquake scenarios, we scale our computations to a case of engineering interest. The case study for the current work is an **M** 6.2 earthquake on the Rose Canyon Fault near San Diego, California (Fig. 1). This fault has been determined (Minster *et al.*, 1999) to be one of the largest sources of seismic hazard in the San Diego area. We choose to analyze an earthquake on the Mission Bay and Del Mar segments of this fault, which are bounded on the north and south by significant changes in strike (Lindvall and Rockwell, 1995). The physical parameters of this fault/earthquake are given in Table 1. For simplicity we model a fault in a homogeneous half-space. Including a low-velocity zone near the surface would of course be more realistic, but we

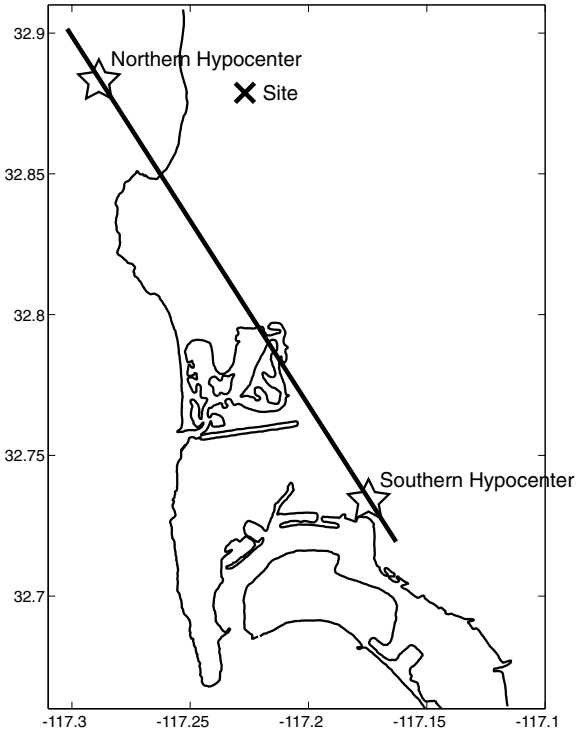

Figure 1. Map of Rose Canyon Fault (thick line) and examined site (cross). The coastline is outlined in black, and the modeled epicenters are marked by stars.

Table 1
Physical and Computational Parameters*

Fault dip	90°
Density	2800 kg/m^3
V_P	6170 m/sec
V_S	3610 m/sec
Static coefficient of friction	0.8
Sliding coefficient of friction	0.5
Fault length (along strike)	24 km
Fault width (vertical)	12 km
Grid spacing	250 m
Critical slip-weakening distance	0.1 m

*After Magistrale (1993).

Table 2
Fault and Station Locations

	Latitude	Longitude
Northern end of fault	32.9015	−117.3020
Southern end of fault	32.7193	−117.1630
Northern hypocenter (depth 6 km)	32.8806	−117.2861
Southern hypocenter (depth 6 km)	32.7402	−117.1789
Examined site	32.8788	−117.2270

are interested in isolating the effects of stress and strength homogeneity from structural effects. Among other effects, a low-velocity zone near the surface would tend to slow down the rupture propagation and amplify ground motion and thus act as somewhat of an envelope applied to the present results. However, we do not expect the relative effects in the current study to change much by the choice of velocity structure. As a case study of how the current method might be used for seismic hazard analysis, we have chosen to examine ground motion at a site near the northern end of the fault (Fig. 1, Table 2), which is approximately 4 km from the closest approach of our simplified fault plane.

Computational Method

We use the 3D finite-difference method of Day (1982) to perform our dynamic faulting simulations. This method uses a slip-weakening coulomb fracture criterion, and nucleation is accomplished by artificially propagating rupture at a fixed (3 km/sec) rupture velocity inside a circle with radius 2.7 km. The computational parameters are given in Table 1. The key difference between the current simulation method and previous studies is the nature of the stress distribution on the fault. Most dynamic faulting studies assume constant normal stress (i.e., constant yield stress) with variable shear prestress (e.g., Day, 1982; Olsen *et al.*, 1997; Nielsen and Olsen, 2000; Peyrat *et al.*, 2001). The assumption that yield stress is constant is often used for simplicity, as well as for lack of any compelling observational reason to choose another pattern. This scenario can be thought of as a limiting or end-member case, in which the relative fault strength, $S = \dfrac{\sigma_y - \sigma_0}{\sigma_0 - \sigma_f}$ (where σ_y is yield stress, σ_0 is initial shear stress, and σ_f is the sliding frictional stress) (Das and Aki, 1977), is strongly linked to the stress drop; highly inhomogeneous stress drop naturally leads to highly inhomogeneous relative fault strength. In contrast, we take an intermediate approach: both shear and normal stress vary, but they have the same spatial variation pattern. In this way, highly inhomogeneous stress drop on the fault can be associated with large or small variations in relative fault strength.

Sample distributions of shear and yield stress are shown in Figure 2. Note that since we assume a simple Coulomb yield criterion ($\sigma_y = |u\sigma_n|$, where μ is the static frictional coefficient and σ_n is the normal stress), yield stress is directly proportional to normal stress. Both shear and yield stresses have the same spatial pattern. However, close inspection shows that the troughs in the yield stress are proportionally slightly higher (in a manner to be explained more fully shortly) than the troughs in the shear prestress. Thus, the low-stress regions are zones of higher relative fault strength (higher S) than the high-stress regions and serve as barriers

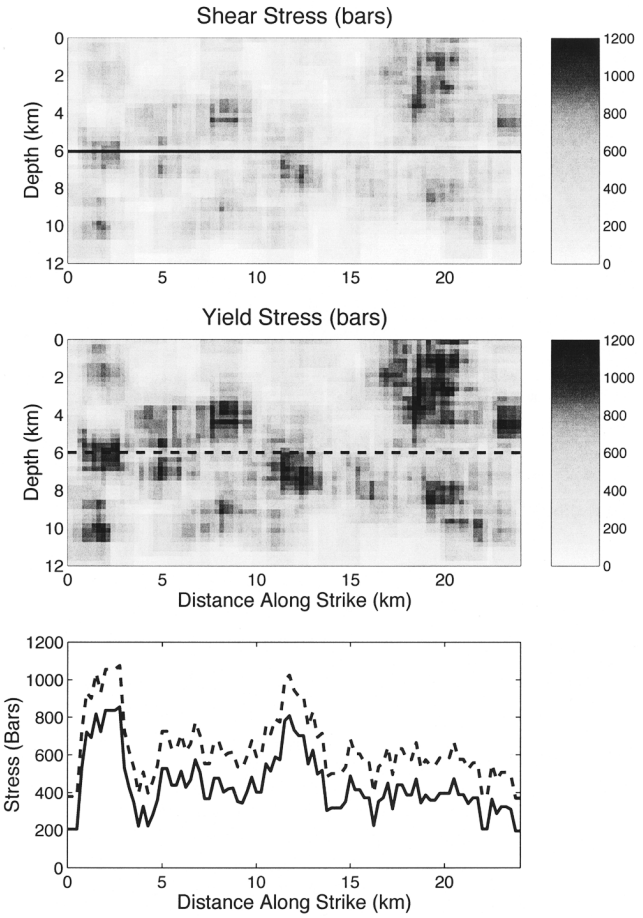

Figure 2. Explanation of relationship between shear stress and yield stress in dynamic models. The top two panels show the shear and yield stresses on the fault plane for one randomization realization of the coarse model. The bottom panel shows the yield stress (dashed) and shear stress (solid) along the lines in the upper panels.

to rupture. Because of this property, the low-stress areas will have a great effect on the propagation of rupture and the development of slip on the fault. This is the same basic situation as if we had chosen a constant yield stress and variable shear stress, except that here we may adjust the relative strength of the barriers independently from the overall stress drop. We should point out that areas of low initial shear stress lead to negative stress drop, a model feature also seen in other studies (e.g., Bouchon, 1997; Ide and Takeo, 1997; Day *et al.*, 1998; Peyrat *et al.*, 2001). One interpretation of these negative stress drop areas is that they are places where previous slip has already relieved stress. However, as we shall see, these locations still often have nonzero slip driven by the surrounding high-stress-drop areas. In the ensuing methodology, we look at three different cases: (1) a case in which the barriers have very high relative strength, referred to as the rough case, (2) a case in which the barriers are not much stronger than the rest of the fault, referred to as the smooth case, and (3) a case with properties intermediate between the two extremes, called the intermediate case. Note that in all these cases, roughness refers to variations in strength on the fault, while in all cases the stress drop is highly inhomogeneous.

Since stress on the fault is not very well constrained observationally prior to an earthquake, we use multiple randomized realizations of fault stress to study the variability of fault rupture, slip, and ground motion. Of particular interest is how the random variability of fault behavior depends on the assumed roughness of the fault strength. In the current models, we assign the random stress field in the following manner: First, we assign a background shear stress level of 0.013 bars to the fault to assure that there would be no areas with zero stress (although the results are quite insensitive to the level of this background stress). Then, we take uniformly distributed random values of stress (between zero and 130 bars) and assign them to random computational nodes on the fault, representing 10% of the fault area. In other words, the along-strike and down-dip coordinates of the concentrated asperity regions are each uniformly distributed random numbers between zero and the maximum extent (along strike and down dip) of the fault. With a nodal spacing of 0.25 km on the fault, this distribution has an average separation of approximately 0.8 km. Then, these stress values are smoothed over a spatial window of 1 km to achieve stress patterns such as the two shown in Figure 3. After assigning shear stress in this way, the normal stress is given the same spatial variability (with a maximum value of 200 bars), meaning that everywhere on the fault the normal stress is directly proportional to the shear stress. At this point, our stress assignment method would give highly inhomogeneous stress drop, but a constant relative fault strength S. Our goal is to produce a variation in S, with S larger in places with low stress drop. Our motivation is to make low-stress barriers, while the high-stress-drop areas will be more prone to rupture. To accomplish this goal, we add an increment to the normal stress in the low-stress areas as the final step in

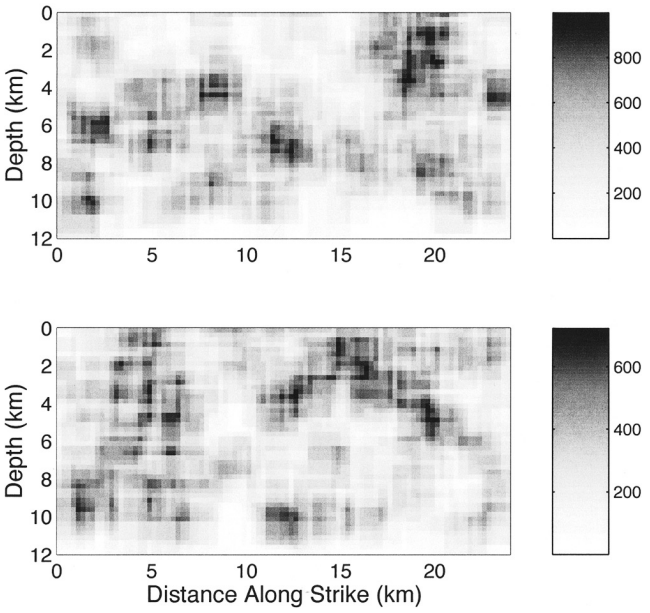

Figure 3. Two different realizations of the random shear stress. Note that although the peak stress values are different between the two realizations, the average stress drop of each is scaled to 30 bars.

model preparation. This added normal stress is proportional to the difference between the local normal stress and its maximum across the entire fault. Put mathematically, the normal stress at a point is incremented by the formula

$$\sigma_n = \sigma_n^0 + \rho(\max(\sigma_n^0) - \sigma_n^0),$$

where σ_n is the final (i.e., to be used in the dynamic model) normal stress at a point, σ_n^0 is the initial (random) normal stress at that point, and maximum is to be taken over the entire fault plane. The constant of proportionality ρ for the added-in increment is different in the rough, intermediate, and smooth cases: In the rough case the proportionality constant is high (0.13), leading to yield stress in the barriers that is high relative to the shear stress. In the smooth case, the constant of proportionality is low (0.05), and in the intermediate case it is in between these extremes (0.10). Finally, the stress distributions are scaled to produce an average stress drop of 30 bars so that the results from different stress distributions may be directly compared. As will be shown later, this scaling also leads to very similar seismic moments and peak velocities among the different stress distributions. The distributions of stress drop and S each influence the dynamics, and the same range of phenomena is not present in models in which only one of these parameters is varied. A qualitative justification for the preceding stress assignment method includes the observation that after an earthquake, the sliding frictional stresses should be roughly proportional to the normal stress on the fault. This could lead to a coupling of the spatial patterns of shear and normal stress that would last until the next earthquake on this fault, moderated by

some sort of aseismic creep or plastic flow that could somewhat smooth out the shear stresses. Regardless of qualitative physical arguments, it is important to note that the preceding recipe is really an *ad hoc* parameterization of the fault plane stresses, without a quantitative theoretical justification. This parameterization permits us to investigate a range of fault behaviors by varying the fault strength and the stress drop independently. As will be shown in the following section, the current scheme produces fault slip and ground motion that are consistent with recent earthquakes and earthquake models.

In addition to different randomized stress distributions, another important variable is hypocentral location. Because our ground-motion site is near the northern edge of the fault, directivity is an important factor in the groundmotion variability at this location. Therefore, we have used two different hypocentral locations as shown in Figure 1 and Table 2. In summary, our study has the following variables: (1) roughness (relative height of barriers on the fault) (2) randomized stress realization, and (3) hypocenter location. We ran 10 simulations for each combination of roughness case and hypocentral location, for a total of 60 different simulations. However, it is significant that in the rough case, only 4 out of 10 southern-hypocenter and 3 out of 10 northern-hypocenter simulations produced slip outside of the nucleation regions; all other ruptures died out shortly thereafter. In the intermediate case, only 5 out of 10 southern-hypocenter and 5 out of 10 northern-hypocenter simulations ruptured the entire fault. In the smooth case, 9 out of 10 southern-hypocenter and 9 out of 10 northern-hypocenter simulations ruptured the entire fault. In the results to follow, we analyze only the four southern-hypocenter and three northern-hypocenter randomization realizations that produced whole-fault rupture for all three smoothness cases. In this way the results of the different smoothness cases may be directly compared.

Results

Fault Dynamics

To facilitate a comparison between our results and a metanalysis of inverted rupture patterns from recent earthquakes (Somerville *et al.*, 1999), we have chosen to display our results in a manner similar to that work. In particular, we follow Somerville *et al.* (1999) by ignoring (in our post-rupture analysis) portions of the fault that have slip less than 0.3 times the average slip on the fault. These parts of the fault are blocked out in white in the figures to follow. Numerical experiments have shown that the average slips, rupture velocities, and other fault properties are not very sensitive to the threshold above. A typical set of rupture time contours for a particular randomized realization of a smooth (low barrier) model is shown in the middle panel of Figure 4a, with the corresponding stress drop pattern for this model in the upper panel. Note that even though the stress pattern is highly inhomogeneous, the relatively homogeneous strength (S) distribution on the fault leads to a largely circular rupture front. We also see faster rupture propagation at the surface due to reflected waves from the free surface. In the intermediate roughness model (Fig. 4b), the rupture front is less circular due to slower rupture propagation in the low stress (and high barrier) regions. The roughest fault model (Fig. 4c) exhibits the least circular rupture front. In this case, the rupture clearly follows the high-stress (and low-strength) regions on the fault, with the rupture front slowing down and almost dying out in the barrier regions (a behavior also observed in the models of Day [1982] and Nielsen and Olsen [2000]).

The noncircular rupture fronts in the rougher models imply that the rupture velocity in these cases is not homogeneous on the fault. This effect can be seen in the bottom panels of Figure 4. The local rupture velocity is calculated by taking the reciprocal of the local gradient of the rupture time. We have blocked out in white the nucleation region (where the rupture velocity is fixed) and the regions of the faults that did not slip (where the rupture velocity is zero). In the smooth case (Fig. 4a), the rupture velocity is relatively homogeneous, with a mean value (across all randomization realizations and hypocenter locations) of 2.72 $\pm$ 0.74 km/sec (the uncertainty given here and henceforth is the standard deviation). In this case the rupture velocity does not show much variation with stress drop but tends to reflect the relatively constant relative strength (S). In the intermediate case (Fig. 4b), the distribution of rupture velocity is more inhomogeneous, with lower rupture velocity in the barrier regions where the stress drop is low and the strength is high. The average rupture velocity for all realizations of this case is 2.20 $\pm$ 0.74 km/sec. The rough case continues the trend of inhomogeneous rupture velocity even farther, with very low rupture velocities in the barrier regions. The mean rupture velocity in this case is 1.84 $\pm$ 0.79 km/sec. It is important to note that the peak rupture velocities in the high-stress-drop/low-strength regions are comparable among the smooth, intermediate, and rough cases. The difference lies in what happens in the barriers, where the slowing down of the rupture leads to the noncircular rupture fronts seen in the rough models.

Another way of viewing the relationship between stress drop and rupture velocity for the three different smoothness cases is shown in Figure 5. This figure shows rupture velocity versus stress drop for all the three different smoothness cases across all randomization realizations and hypocenter locations, with the results partitioned in 0.2 km/sec bins in velocity and 2-bar bins in stress drop. The darkness of the plot corresponds to the relative number of points in that bin. There is a correlation between rupture velocity and stress drop for all three cases (correlation coefficients of 0.2322, 0.2204, and 0.0458 for the smooth, intermediate, and rough cases, respectively), and as expected, this correlation decreases with the smoothness of the fault. However, the plots in Figure 5 show a more complicated relationship among

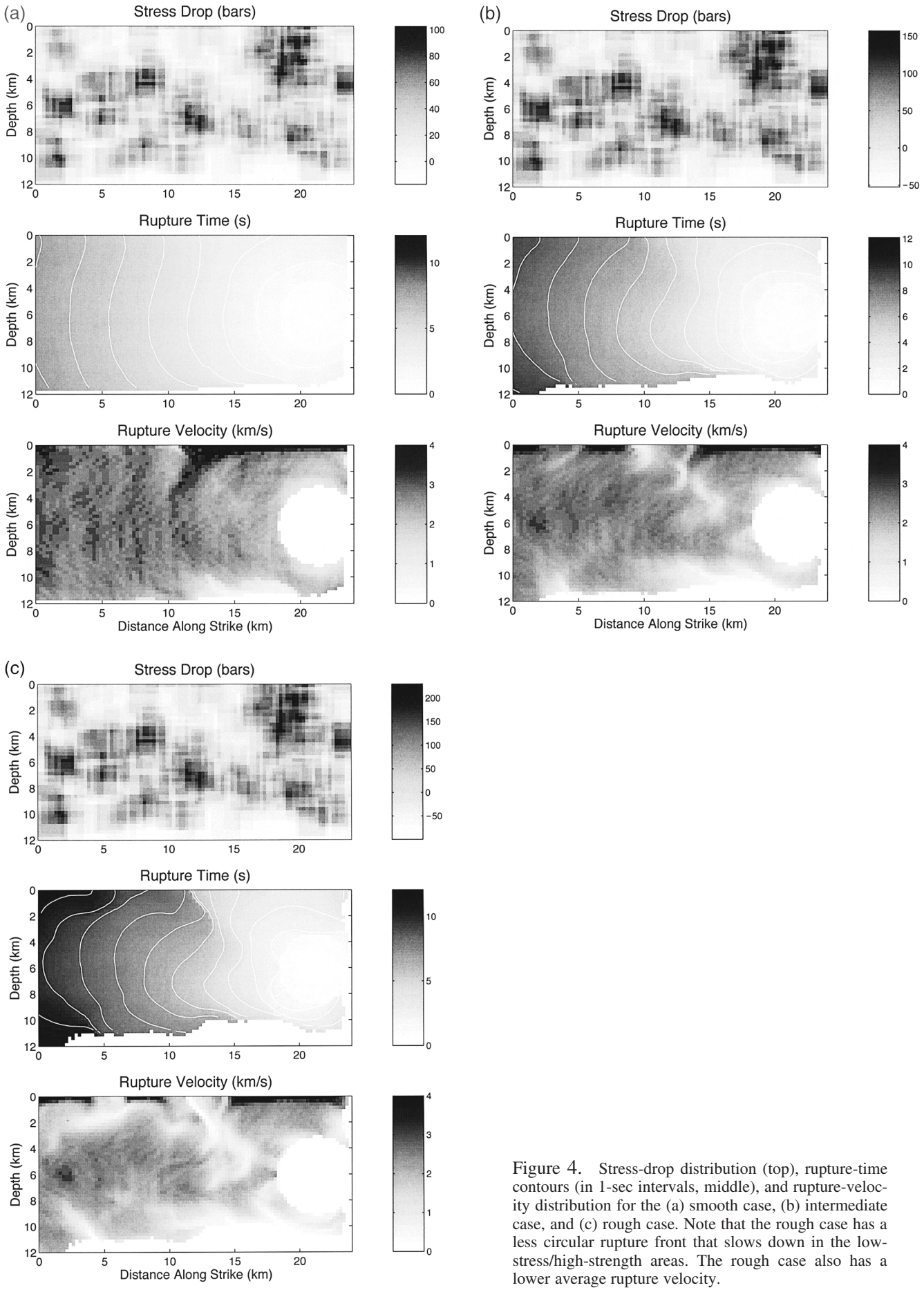

Figure 4. Stress-drop distribution (top), rupture-time contours (in 1-sec intervals, middle), and rupture-velocity distribution for the (a) smooth case, (b) intermediate case, and (c) rough case. Note that the rough case has a less circular rupture front that slows down in the low-stress/high-strength areas. The rough case also has a lower average rupture velocity.

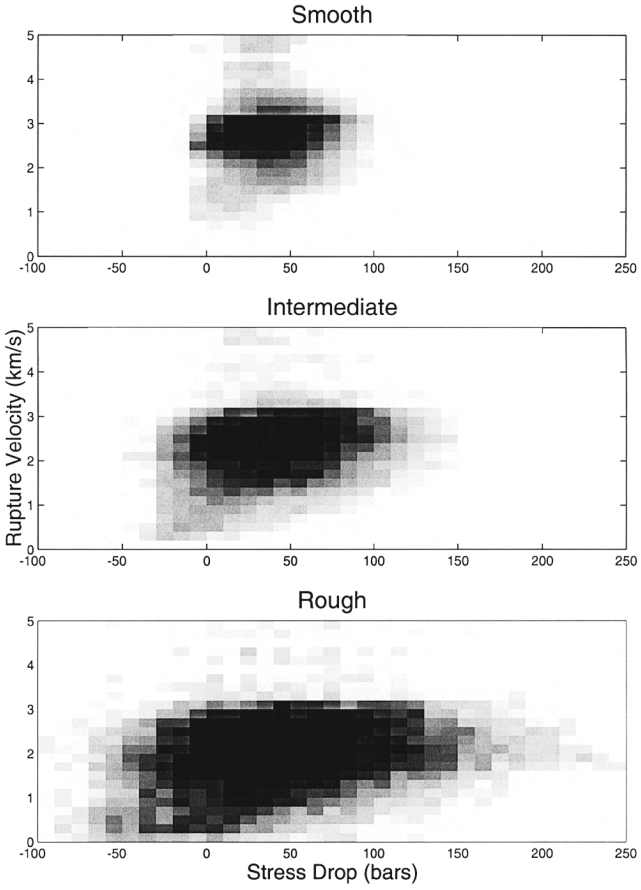

Figure 5. Plots of rupture velocity versus stress drop for the smooth (top), intermediate (middle), and rough (bottom) cases. Each plot has a point for every node on the fault outside the nucleation zone with nonzero slip, corresponding to 27,374 points for the smooth case, 25,557 points for the intermediate case, and 22,527 points for the rough case. The results are partitioned in 0.2 km/sec bins in velocity and 10-bar bins in stress drop, with the darkness the plot corresponding to the relative number of points on the fault with rupture velocity and stress drop in that bin. There is a small correlation between rupture velocity and stress drop for all cases, but the relationship is quite complicated (see text).

these quantities. In all three cases (although it is most obvious in the rough and intermediate cases), we see that most rupture velocities lie below the Rayleigh-wave speed for this medium, which is approximately 3.3 km/sec. There are outliers of higher velocity, which are due to either the rupture front jumping ahead (to the *P*-wave velocity) in various regions, especially near the free surface, or to the near-instantaneous rupture of a section of the fault after having been loaded up by rupture in surrounding regions. The former behavior is more common in the smooth model, leading to a higher average rupture velocity. The latter behavior is more common in the rough model, leading to both high and low outliers. As shown in Figure 5, though, the correlation coefficient does not adequately describe the relationship between rupture velocity and stress drop. This relationship might be more accurately described as providing an envelope for the rupture velocity at a point, which is further varied by a number of dynamic effects including the entire history of slip on the fault prior to the point's rupture. As shown subsequently, the differences in average rupture velocity among the model cases has great importance for the development of directivity pulses for points on the surface.

Sample rise-time distributions for the smooth, intermediate, and rough cases are shown in the middle panels of Figure 6. Rise time at a point is calculated by finding the time at which 90% of the cumulative squared velocity for that point has arrived. The slip duration (rise time) is the difference between this time and the recorded rupture time for that point. The nucleation region and the regions that did not slip can bias the rise-time calculation because the rupture propagation is predetermined in the nucleation region and is nonexistent in the unslipped regions. Thus, these areas are not displayed, as in Figure 4. As in the case of the rupture velocity, the connection between rise time and stress drop is rather complicated. In the smooth case (Fig. 6a), rise times are high ($>$1 sec) over much of the fault. High-stress-drop regions appear to have lower rise times. This effect is likely because of healing phases radiated off the edges of the barriers. The intermediate case (Fig. 6b) shows more spatial variation in rise time, although here again low rise times appear to be associated with high-stress-drop and low-strength regions. Because there is a greater strength contrast, healing pulse generation is consequently more efficient, leading to slightly shorter rise times. More importantly, this effect leads to more local control of the slip duration, and thus higher rise-time inhomogeneity. The rough case (Fig. 6c) continues this trend. Rise times are highly inhomogeneous, and the association of high-stress-drop/low-strength regions with low rise time is even more pronounced.

Figure 7 shows the relationship between rise time and stress drop for the smooth, intermediate, and rough cases, across all hypocenter and randomization realization combinations. This plot is similar to Figure 5, except with rise time plotted versus stress drop. As implied by inspection of Figure 6, rise time is negatively correlated with stress drop, with the smooth case having the weakest correlation. Correlation coefficients are -0.1884, -0.2707, and -0.2391, respectively. However, the dependence of rise time on stress drop is even more complicated than the dependence of rupture velocity on stress drop. Figure 7 shows that at a given stress drop there is a maximum value for the rise time (decreasing with increasing stress drop), with a distribution of rise times less than this maximum value. This is especially true for the smooth case. For the rougher cases there are an increasing number of outliers, which are likely due to the way that rise time is calculated in our models—if the slip at a point is very small, the time of slip termination is difficult to define and can lead to artificially high rise times for these points. The effect of these outlying values has a great effect on the average rise times for each of the roughness cases, as seen by

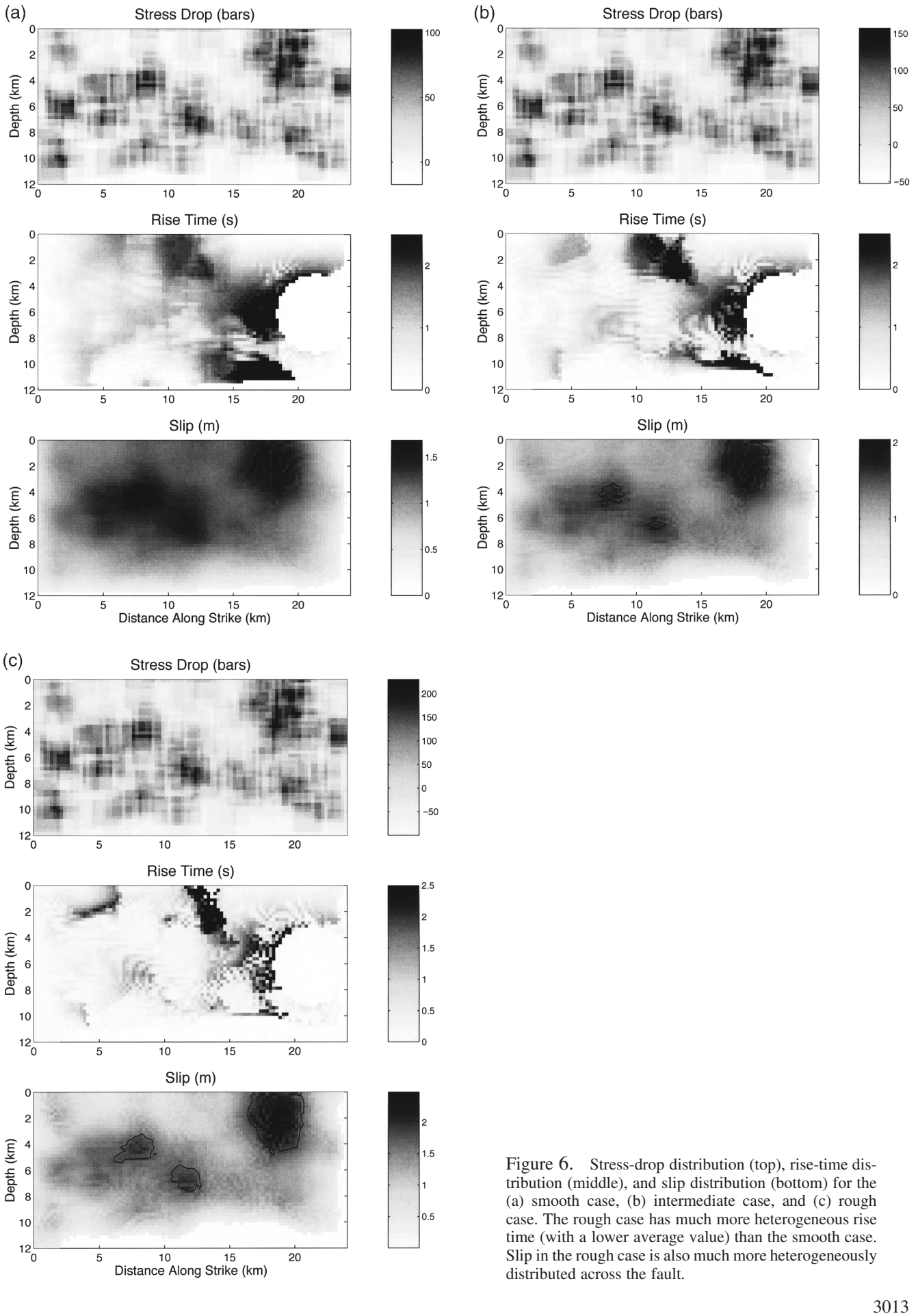

Figure 6. Stress-drop distribution (top), rise-time distribution (middle), and slip distribution (bottom) for the (a) smooth case, (b) intermediate case, and (c) rough case. The rough case has much more heterogeneous rise time (with a lower average value) than the smooth case. Slip in the rough case is also much more heterogeneously distributed across the fault.

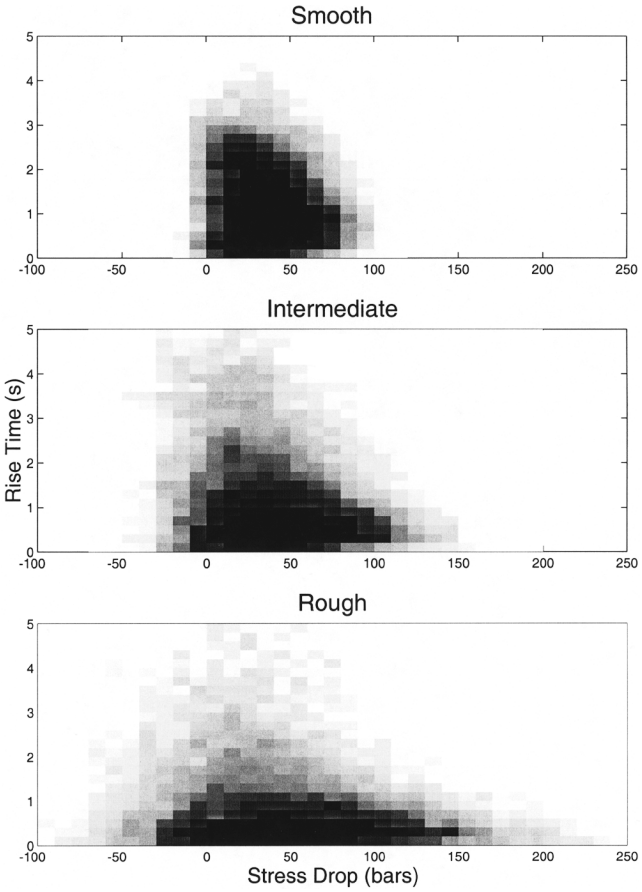

Figure 7. Scatter plots of rise time (slip duration) versus stress drop for the rough (top), intermediate (middle), and smooth (bottom) cases. The same number of points is used as in Figure 5. The results are partitioned in 0.2-sec bins in rise time and 10-bar bins in stress drop, with the darkness the plot corresponding to the relative number of points on the fault with rupture velocity and stress drop in that bin. The stress drop appears to control the maximum possible rise time, which decreases with increasing stress drop.

the difference between mean and median values. The mean (across all hypocentral locations and randomization realizations) rise times for the smooth, intermediate, and rough cases are 1.16 ± 0.80 sec, 1.13 ± 1.14 sec, and 1.17 ± 1.82 sec, respectively. Taken at face value, these numbers would imply that there is no significant difference between the average rise times of the different roughness cases and that the only difference is much greater rise-time variability in the rough case. However, the median values, which are much less sensitive to the high rise-time outliers, tell a different story: the median rise times for the smooth, intermediate, and rough cases are 1.00 sec, 0.72 sec, and 0.50 sec, respectively, displaying a strong decrease in rise time with increasing roughness. It should be pointed out that rise time is the only parameter that has a significant difference between the mean and median values. Since the outlying high rise-time values on the rough fault are in general associated with points with very low slip, they do not contribute very much to the ground motion and would not be resolved in a slip inversion. Therefore, we believe that the median values of rise time more legitimately express the relationship between rise time and fault roughness. In other words, rough faults have much lower rise times (over most of the fault) than smooth faults over most of the fault plane, leading to more localized control of the rupture process and more inhomogeneous slip. This behavior is seen clearly in Figure 7, where the high-density regions in rise-time/stress-drop space shift to lower rise times for the rougher models.

The effect of the fault roughness on the final slip distribution is also quite pronounced. The lower panel of Figure 6a shows the slip for the smooth case. Although there is a correlation between high stress drop and high slip, the slip distribution is much smoother than the stress distribution: slip can leak out of the high-stress-drop regions due to the low barrier strength. Furthermore, as noted before, there is slip even in regions with negative stress drop. Figure 6b shows that the slip distribution for the intermediate case is much more heterogeneous than in the smooth case. Note that for the slip distributions, the gray-scale mapping is scaled to the peak slip on the fault in order to emphasize that the differences among the roughness cases lie in the heterogeneity of slip, not just in its magnitude. The increased heterogeneity in slip is consistent with the more heterogeneous (and lowered) rise time in the intermediate case and the resulting local control of slip. The rough case (Fig. 6c) exhibits even more heterogeneous slip, with concentrations that almost exactly track the high-stress/low relative strength regions. One should also note that the high-slip regions are also the regions with the lowest rise times, implying very high slip rates in these locations. This effect has also been seen in fault-slip inversions such as of Oglesby and Archuleta (1997), as well as the dynamic models of Olsen *et al.* (1997). However, this effect is opposite to the results of Beroza and Mikumo (1996). For brevity we do not show plots of slip versus stress drop but merely note that such plots display features similar to those of the other fault properties, including a positive correlation between slip and stress drop, and the stress drop determining a maximum value for slip, but with a large distribution of slips below this maximum value.

It is possible to arrive at a somewhat quantitative measurement of slip heterogeneity by analyzing the area taken up by asperities, or places with slip above a specified threshold. This measure is not ideal because it does not capture the slip heterogeneity that results from very small patches with very high slip. For example, a uniform slip model and a delta function slip model are two extremes of roughness, yet both would have zero asperity area under any threshold criterion of this type. However, this criterion does allow us to arrive at a number that we may compare with the results of kinematic inversions (Somerville *et al.*, 1999) later in this work. We use a threshold similar to that of Somerville *et al.* (1999), where an asperity is defined as a region with slip at

least 1.5 times larger than the average slip over the fault. Sample asperity regions are outlined in black on the bottom panels of Figure 6. We find that the mean (across all hypocentral locations and randomization realizations) percentage of the fault taken up by asperities is 3.8 ± 2.7% for the smooth case, 6.5 ± 2.0% for the intermediate case, and 8.4 ± 1.8% for the rough case. This quantitative measurement is in agreement with the qualitative observation that slip inhomogeneity is greater for the rough faults.

Figure 8 compares the slip distributions for two stress distribution realizations for the smooth (Fig. 8a) and rough (Fig. 8b) cases. Note that the slip distributions for the smooth case are rather similar, with high slip (varying by only 20% or so) over much of the fault plane, whereas the slip distributions for the rough cases are quite dissimilar, with slip strongly concentrated in the high-stress/low-strength patches. Different randomized stress realizations produce similar effects in the rupture time, rupture velocity, and rise-time distributions. The similarity (in both slip and rupture propagation) among different smooth events and the dissimilarity between different rough events have implications for the predictability of ground motion to be discussed in the

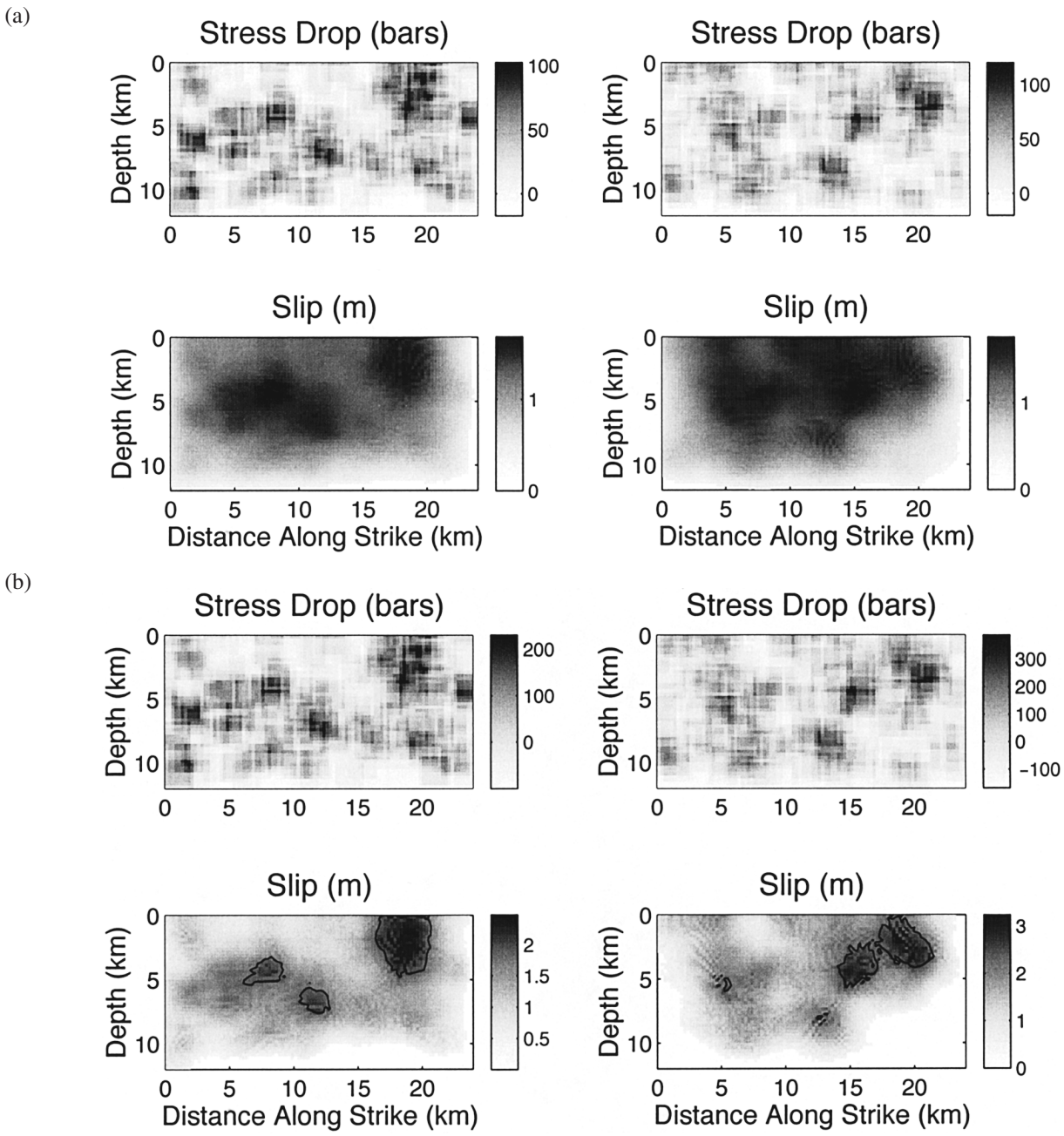

Figure 8. Comparison of the slip from two different randomized stress realizations in (a) the smooth case and (b) the rough case. Slip is much more dependent on the randomized stress distribution in the rough case than in the smooth case.

next section. In spite of the differences between the smooth and rough cases in the distribution of fault motion, the mean seismic moments of all three cases are similar: $1.21 \pm 0.02 \times 10^{19}$ N m for the smooth case, $1.30 \pm 0.06 \times 10^{19}$ N m for the intermediate case, and $1.44 \pm 0.16 \times 10^{19}$ N m for the rough case.

Ground Motion

Up to this point we have concentrated on the effects of fault roughness on the evolution of rupture and slip on the fault. It is also important to explore the implications of roughness assumptions on ground motion. In particular, the effect of the fault dynamics is felt quite strongly in the development of the near-source directivity pulse, which is of crucial importance in engineering applications. The previous results have shown that rougher faults have slower overall rupture propagation, with rupture fronts that speed up and slow down depending on the local fault strength. This effect should tend to lessen the development of a directivity pulse near the fault. To test this hypothesis, we have plotted the horizontal particle velocity for the examined site in Figure 9. In this case and in all ground-motion plots, the synthetics are low-pass filtered with an upper corner frequency of 1.0 Hz. We display separately the ground motion for the two hypocenter locations, the three roughness cases, and for multiple randomization realizations. The number of randomization realizations shown is limited by the number of randomization realizations that produced self-sustaining ruptures in the rough case: Out of 10 randomization realizations, only four ruptures with southern hypocenters and three ruptures with northern hypocenters propagated over the entire fault plane. Thus, for comparison, only those randomization realizations are displayed for all cases. The effect of directivity is seen in all three roughness cases as a strong positive pulse in the early part of the southern-hypocenter strike-perpendicular records. This pulse is almost entirely absent in the northern-hypocenter records, as is expected from the position of the site near the northern end of the fault. The directivity pulse is also much less obvious in the strike-parallel records, also as expected, both from elementary theoretical considerations and from empirical studies (e.g., Somerville *et al.*, 1997). As in the fault motions, there are important differences among the different roughness cases. Reflecting the similar rupture propagation and slip distribution patterns for the smooth cases, the different randomization realizations produce very similar ground motion at our site. Thus, these ground motions essentially record the effect of the fault geometry (its shape, size, and location with respect to the site) and do not show a strong effect of the stress pattern on the fault. In contrast, the intermediate and rough cases show increasing differences among different randomization realizations, with the rough case having very dissimilar ground motions in different runs. Here the effect of the stress pattern on the fault appears to dominate the effect of the fault geometry.

As a measure of the directivity in the ground motion, we took the mean strike-perpendicular peak velocity for the southern-hypocenter runs and divided it by the corresponding mean peak velocity for the northern-hypocenter runs. This directivity factor has a value of 3.97 for the smooth case, 2.97 for the intermediate case, and 2.07 for the rough case. Another measure of directivity more commonly used in engineering applications is the ratio of the peak strike-perpendicular velocity to the mean of the two horizontal-velocity components. To calculate this number, the mean of the two horizontal peak velocities is first calculated, divided into the peak strike-perpendicular ground velocity, and then averaged over randomization realizations. By this measure, the directivity amplification of the strike-perpendicular ground velocity from the southern hypocenter is 1.23 for the smooth case, 1.08 for the intermediate case, and 1.05 for the rough case. The corresponding numbers for the northern hypocenter are 0.54, 0.57, and 0.71, respectively. Regardless of the measure used, it is clear the smooth case has more of a directivity effect than do the intermediate and rough cases. The effect of fault roughness on directivity can also be easily seen in Figures 10 and 11. Figure 10 shows the mean peak strike-perpendicular velocity in the near-source region for all three cases and both hypocenter locations. Here again we average the same randomized realization patterns for all three cases, so the results can be directly compared. In the smooth case, the forward directivity lobe can easily be seen for both the northern and southern hypocenter. This lobe decreases in size in the intermediate case and is quite small in the rough case, showing the strong decrease in directivity with fault roughness. Figure 11 displays the mean ratio of the peak strike-perpendicular velocity to the mean horizontal peak velocity and thus is a surface map of the numbers quoted above for the particular case of our site. As in the previous figure, the lobe of high directivity decreases in size with fault roughness. We also see that the ratio ranges from less than 0.6 to almost 2.0 depending on the location—numbers that we may compare with other studies in the discussion section.

Discussion

The aforementioned results show that rough fault models differ greatly from smooth models. These differences can partly be thought of as aspects of the issue of global (whole-fault) or local control of the rupture process. In the smooth models, the rupture front proceeds rapidly over the fault plane and allows more of the fault to slip simultaneously. The generation of healing phases is weak, leading to a communication between different parts of the fault. Signals from other parts of the fault allow the slip to leak out of the high-stress regions, leading to a more global control of the rupture process. This configuration is very similar to a standard crack model (e.g., Kostrov, 1964). In contrast, the rough fault models have a rupture front that accelerates and decelerates as it propagates over the fault plane. Healing phase generation is strong, and different parts of the fault do not

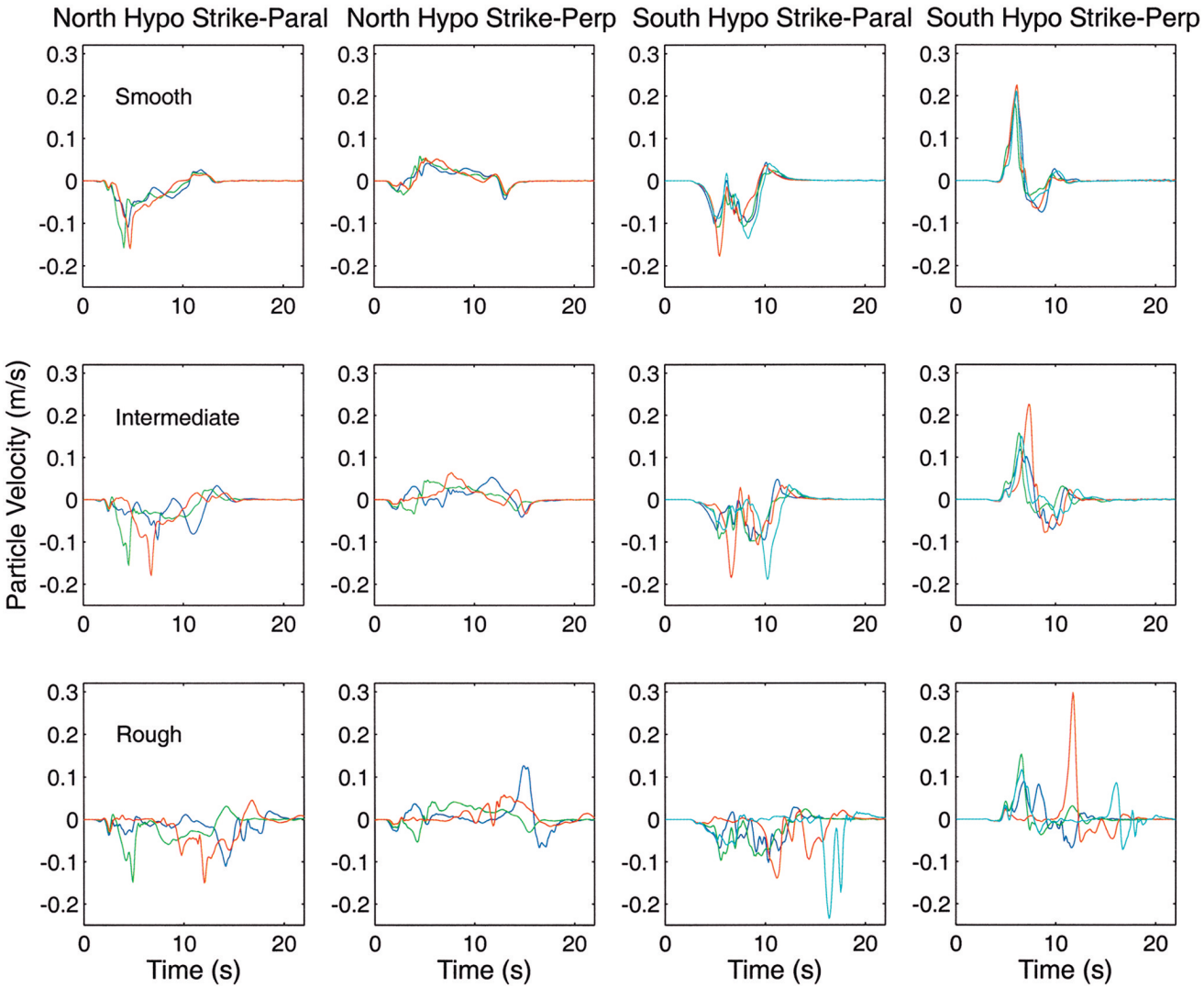

Figure 9. Strike-perpendicular velocity synthetics for multiple randomized stress realizations (different colors), both hypocenter locations (left and right of figure), and the smooth, intermediate, and rough cases (top, middle, and bottom of figure). The smooth case has very similar ground motion for different randomized stress realizations and a strong directivity pulse. The rough case has highly variable ground motion, as well as a less-developed directivity pulse.

communicate with each other, resulting in more local control over the rupture process, with the local stress drop controlling the slip. The result is lower, more heterogeneous rise times and more heterogeneous slip, behaviors that might also be expected of a self-healing or slip-rate-weakening model (Heaton, 1990) that would (unlike our model) have a form of strength recovery in the friction law. In our case, the interpretation is that strength heterogeneity localizes the relationship between fault stress changes and slip, with no rate weakening required to produce the aforementioned effects. This effect has been seen in the work of Day (1982), Beroza and Mikumo (1996), and Day *et al.* (1998). Also contributing to the slip heterogeneity, though, is the additional effect that the stress drop in the rough cases is more heterogeneous than in the smooth cases and thus would produce more heterogeneous slip even in the absence of the dynamic effects described previously. The final slip heterogeneity is due to the sum of the two previously mentioned effects above.

An important feature of the rough models is that the rupture front must tunnel through barriers in which the rupture is not energetically favored. Thus, the rupture front must be fed elastic energy from other parts of the fault for it to propagate through these regions. If the barriers are too strong or too large, the rupture dies out. This happens in the majority of the rough randomization realizations, implying that with this particular set of parameters, the faults are right on the boundary (in phase space) between rupture and stability. In this sense, the rough models are similar to Nielsen and Olsen's (2000) dynamic model for the 1994 Northridge

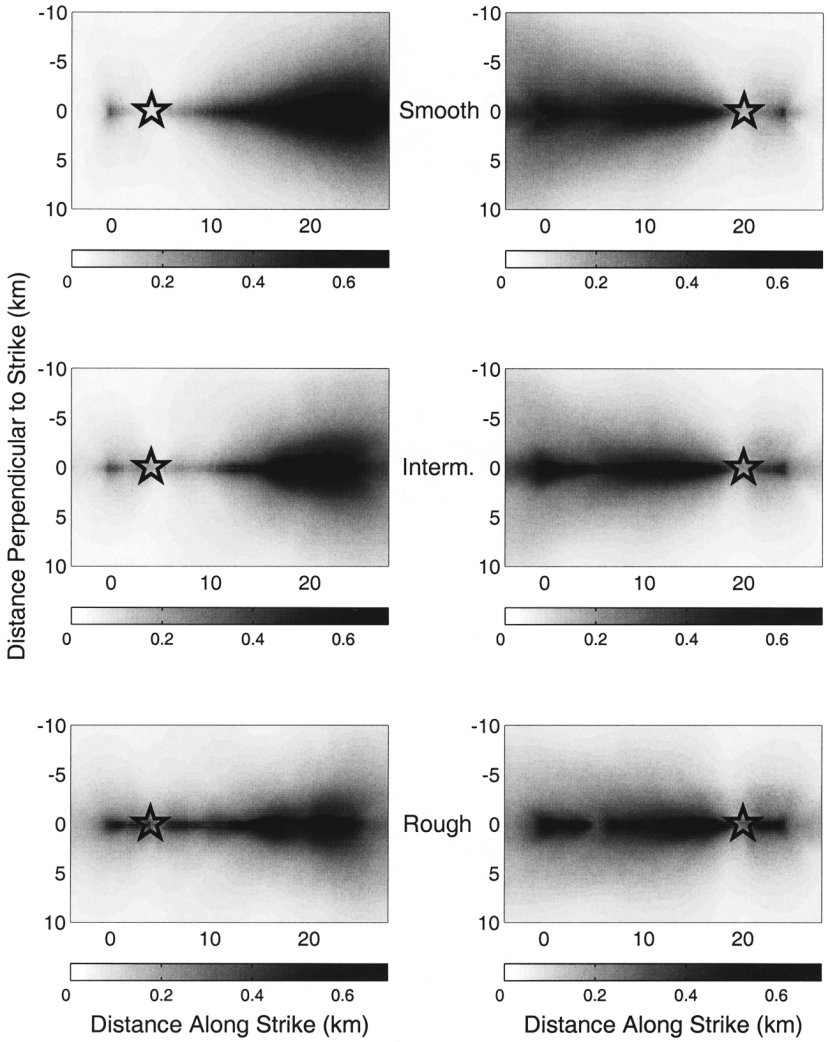

Figure 10. Comparison of average (across all randomization realizations) peak ground velocity in the near-source region for the northern hypocenter (left side) and southern hypocenter (right side) in the smooth (top), intermediate (middle), and rough (bottom) cases. The epicenter is marked with a star. There is a well-developed directivity lobe for the smooth case but much less of one for the rough case.

earthquake and Madariaga and Olsen's (2000) model for the 1992 Landers earthquake, in which only very finely tuned stress patterns could produce rupture over the entire fault plane and still produce sufficient slip heterogeneity to match inverted slip patterns. This effect has also been noted in Olsen *et al.* (1997) and Peyrat *et al.* (2001).

The ground-motion calculations resulting from the current earthquake models serve two functions: to help indicate which type of model is more applicable to the real world, and to provide sample ground-motion calculations that could be used in seismic hazard analysis. To address the former function, we can compare the slip heterogeneity and ground-motion directivity to observational studies. As stated above, the mean percentage of the fault inside an asperity (with slip 1.5 times the mean slip on the fault) is 3.8 $\pm$ 2.7% for the smooth case, 6.5 $\pm$ 2.0% for the intermediate case, and 8.4 $\pm$ 1.8% for the rough case. Somerville *et al.* (1999), applying a similar measurement of asperity area to a number of recent inverted fault models, find a range of asperity area percentages from around 5% to 40%, with a mean of 22%. All of our roughness cases have asperity areas substantially smaller than the mean asperity area of Somerville *et al.* (1999), leading to the conclusion that our model still does not adequately reproduce the slip heterogeneity found in nature (although the definition of Somerville *et al.* [1999] is more complicated than ours, so the comparison is not ideal). This observation is especially true when one considers that most slip inversions have a smoothness constraint as an assumption; thus, the slip heterogeneity in the inverted slip models can be viewed as a lower bound to the true heterogeneity. However, the results do suggest that the rough case is the case most consistent with the slip heterogeneity data.

Another result that we may compare with observation is the directivity effect in our synthesized ground motions. Using multiple source-receiver geometries, Somerville *et al.* (1997) arrived at a typical amplification value of 1.5 for the ratio of the peak strike-perpendicular velocity to the average of the two horizontal components. Our amplification factors of 1.23 for the smooth case, 1.08 for the intermediate case, and 1.05 for the rough case are significantly smaller. However, as can be seen in Figure 11, the ratio in our models does extend to 1.5 and is significantly more than 1.25 for a

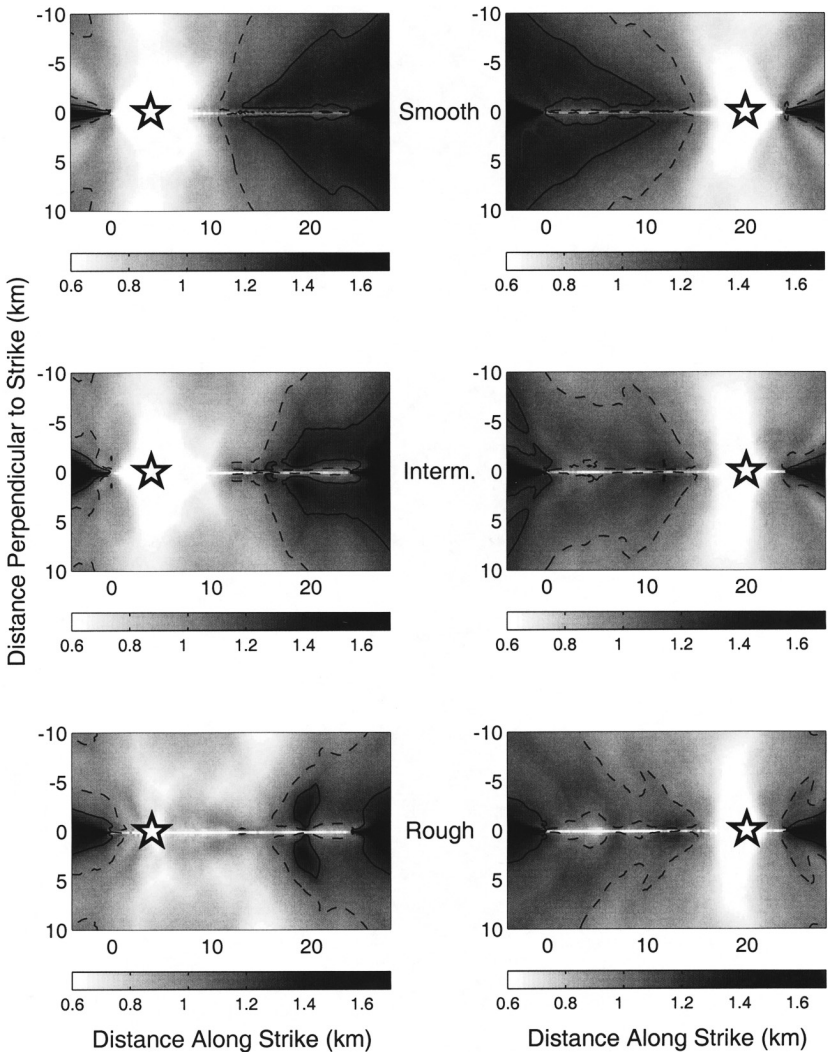

Figure 11. Comparison of average (across all randomization realizations) ratio of peak strike-perpendicular velocity to mean horizontal peak velocity in the near-source region for the northern hypocenter (left) and southern hypocenter (right) in the smooth (top), intermediate (middle), and rough (bottom) cases. The dashed contour corresponds to a ratio of 1.0, and the solid contour corresponds to a ratio of 1.25. The epicenter is marked with a star. The area with high ratio decreases as fault roughness increases, as does the maximum value of the ratio, indicating a decrease in directivity with increasing fault roughness.

great deal of the near-fault area in the smooth case but not in the rough case. Thus, it appears that the smooth case produces directivity effects that are most comparable (over a greater area near the fault) with ground motion from actual earthquakes. It should be pointed out that the current results do not contradict the results of Boore and Joyner (1978), who found that heterogeneity in rupture velocity amplified rather than attenuated directivity effects. Their study compared kinematic models that had the same average rupture velocity but different degrees of rupture velocity heterogeneity. In our study, the main effect on directivity is largely due to the differences in average rupture velocity between the rough and smooth cases. Furthermore, Boore and Joyner (1978) also showed that heterogeneous slip also tended to increase rupture directivity. This effect works against the effect that rupture velocity decreases with fault roughness, and thus may reduce the significance of the effect of fault strength roughness on directivity.

There are additional comparisons that one can make with real earthquakes. The mean rupture velocity for the smooth case is closer to the Rayleigh-wave velocity of the medium and thus is perhaps closer to what one would expect in a real earthquake (although local supershear rupture velocities may well be possible in real earthquakes, such as the 1979 Imperial Valley event [Archuleta, 1984] and 1999 Izmit, Turkey, event [Bouchon *et al.*, 2001]). However, even in the rough case, the rupture velocity in the high-slip areas (which would contribute most to a rupture history inversion) also have rupture velocities comparable to the smooth case. On balance, rupture velocity and directivity appear more realistic in the smooth models, whereas asperity area tends to favor rougher models. Whereas these comparisons with observational evidence are in this sense inconclusive, it should be kept in mind that we have used a particular parameterization of the stress drop and barrier strength in all these models. We have only explored a very small section of parameter space; there is clearly no guarantee that the current models are anywhere near the best possible. In particular, there is the possibility that a more complicated rate-weakening or rate-and-state friction law (i.e., one with intrinsic restrengthening) could produce a better simultaneous fit to the slip heterogeneity, rupture velocity, and directivity,

as was seen by Nielsen and Olsen (2000). Rate weakening, due to restrengthening in the friction law, might lead to shorter rise times and greater slip heterogeneity, while still giving a more uniform rupture velocity and a resultant higher directivity effect. Alternatively, using a different correlation length in forming the stress patterns could greatly change the results of this study and perhaps lead to a result closer to that of Beroza and Mikumo (1996), who suggest that rate weakening is not needed to explain some of these effects. Such models are the scope of future work.

Conclusions

The present work serves to delineate the effects of certain assumptions about the stress drop and strength distributions on faults. In particular, by varying the roughness (relative barrier strength) on faults, we can see the transition between a more homogeneous, globally controlled dynamic regime to one that is more inhomogeneous and locally controlled. Compared to smooth faults, rough faults have (1) slower and more inhomogeneous rupture velocities (with locally fast rupture propagation in high-stress patches), (2) smaller and more heterogeneous rise times, (3) more heterogeneous slip, (4) more variable ground motion (between different randomization realizations), and (5) smaller directivity effects. Slip inversions of recent earthquakes do not conclusively discriminate among the various models of fault roughness. Experiments with different strength parameterizations and friction laws may help clear up this issue, and the issues raised by limited resolution of the inversions themselves may need to be considered as well. Regardless, the trends listed are expected to apply regardless of the fine details of the friction law used.

In all cases, rupture velocity, rise time, and slip are associated with the fault strength and stress drop, as well as each other. For purposes of seismic hazard forecasting, it would be desirable to modify kinematic models (which largely assume that these values are not correlated) to reflect the associations seen in the present dynamic models. However, as has been shown in the current work, the connections between these quantities are not simple ones—the relationships are more like an envelope than a simple correlation. It is thus not obvious how a rule-based kinematic modeling scheme could reflect these connections. Perhaps the most valid way to proceed would be to simply use the current stochastic-stress technique (perhaps with different assumptions about fault stress and strength) to produce ground motions directly, without using a kinematic modeling step. A final alternative would be to produce a suite of dynamic rupture models using a stochastic-stress method, and then use kinematic techniques and simpler wave propagation models to propagate the synthetic ground motions to the locations of interest. In any of these cases, the result will be a more physically based estimate of ground motion for seismic hazard calculations.

Acknowledgments

This manuscript was greatly improved by the thoughtful reviews of Kim Olsen and Paul Somerville, as well as useful conversations with Martin Mai. This research was funded by National Science Foundation Grant CMS-99800663 and the Southern California Earthquake Center (SCEC). SCEC is funded by NSF Cooperative Agreement EAR-8920136 and USGS Cooperative Agreements 14-08-0001-A0899 and 1434-HQ-97AG01718. The SCEC Contribution Number for this article is 680.

References

Archuleta, R. J. (1984). A faulting model for the 1979 Imperial Valley earthquake, *J. Geophys. Res.* **89,** 4559–4585.

Beroza, G. C., and T. Mikumo (1996). Short slip duration in dynamic rupture in the presence of heterogeneous fault properties, *J. Geophys. Res.* **101,** 22,449–22,460.

Boore, D. M., and W. B. Joyner (1978). The influence of rupture incoherence on seismic directivity, *Bull. Seism. Soc. Am.* **68,** 283–300.

Bouchon, M. (1997). The state of stress on some faults of the San Andreas System as inferred from near-field strong motion data, *J. Geophys. Res.* **102,** 11,731–11,744.

Bouchon, M., M.-P. Bouin, H. Karabulut, M. N. Toksoz, M. Dietrich, and A. J. Rosakis (2001). How fast is rupture during an earthquake? New insights from the 1999 Turkey earthquakes, *Geophys. Res. Lett.* **28,** 2723–2726.

Das, S., and K. Aki (1977). Fault plane with barriers: a versatile earthquake model, *J. Geophys. Res.* **82,** 5658–5670.

Day, S. M. (1982). Three-dimensional simulation of spontaneous rupture: the effect of nonuniform prestress, *Bull. Seism. Soc. Am.* **72,** 1881–1902.

Day, S. M., Y. Guang, and D. J. Wald (1998). Dynamic stress changes during earthquake rupture, *Bull. Seism. Soc. Am.* **88,** 512–522.

Fukuyama, E., and R. Madariaga (2000). Dynamic propagation and interaction of a rupture front on a planar fault, *Pageoph* **157,** 1959–1979.

Heaton, T. (1990). Evidence for and implications of self-healing pulses of slip in earthquake rupture, *Phys. Earth Planet Interiors* **64,** 1–20.

Ide, S., and M. Takeo (1997). Determination of constitutive relations of fault slip based on seismic wave analysis, *J. Geophys. Res.* **102,** 27,379–27,391.

Kostrov, B. V. (1964). Self-similar problems of propagation of shear cracks, *J. Appl. Math. Mech.* **28,** 1077–1087.

Lindvall, S. C., and T. K. Rockwell (1995). Holocene activity of the Rose Canyon fault zone in San Diego, California, *J. Geophys. Res.* **100,** 24,121–24,132.

Madariaga, R., and K. B. Olsen (2000). Criticality of rupture dynamics in 3-D, *Pageoph* **157,** 1981–2001.

Magistrale, H. (1993). Seismicity of the Rose Canyon fault zone near San Diego, California, *Bull. Seism. Soc. Am.* **83,** 1971–1978.

Mai, P. M., M. Guatteri, G. C. Beroza, and J. Boatwright (2001). Toward a more physical basis for strong-motion simulation, *Seism. Res. Lett.* **72,** 273.

Minster, B., J. Wagoner, R. Mellors, S. Day, S. Park, S. Elrick, F. Vernon, and F. Heuze (1999). Initial source and site characterization studies for the U. C. San Diego Campus, Lawrence Livermore National Laboratory Technical Report—UCRL-ID-134785, Livermore, California.

Nielsen, S. B., and K. B. Olsen (2000). Constraints on stress and friction from dynamic rupture models of the 1994 Northridge, California, earthquake, *Pageoph* **157,** 2029–2046.

Oglesby, D. D., and R. Archuleta (1997). A faulting model for the 1992 Petrolia earthquake: can extreme ground acceleration be a source effect? *J. Geophys Res.* **102,** 11,877–11,897.

Olsen, K. B. R. Madariaga, and R. J. Archuleta (1997). Three-dimensional dynamic simulation of the 1992 Landers earthquake, *Science* **278,** 834–838.

Peyrat, S., K. B. Olsen, and R. Madariaga (2001). Dynamic modeling of the 1992 Landers earthquake, *J. Geophys Res.* **106,** 26,467–26,482.

Somerville, P. G., K. Irikura, R. Graves, S. Sawada, D. Wald, N. Abrahamson, Y. Iwasaki, T. Kagawa, N. Smith, and A. Kowada (1999). Characterizing crustal earthquake slip models for the prediction of strong ground motion, *Seism. Res. Lett.* **70,** 59–80.

Somerville, P. G., N. F. Smith, R. W. Graves, and N. A. Abrahamson (1997). Modification of empirical strong ground motion attenuation relations to include the amplitude and duration effects of rupture directivity, *Seism. Res. Lett.* **68,** 199–222.

Department of Earth Sciences
University of California, Riverside
Riverside, California 92521
(D.D.O.)

Department of Geological Sciences
San Diego State University
550 Campanile Drive
San Diego, California 92182
(S.M.D.)

Manuscript received 20 September 2001.